The effect of the wall slip on the stability of the Rayleigh-Bénard Poiseuille flow for viscoplastic fluids

Christel METIVIER[a], Albert MAGNIN[a]

a. *Laboratoire de Rhéologie - UMR* 5520 *(CNRS - Grenoble-INP - UJF)*
1301, rue de la piscine - BP 53 - 38041 *Grenoble Cedex*

Résumé :

Une analyse linéaire de stabilité de l'écoulement de Rayleigh-Bénard Poiseuille est réalisée pour un fluide de Bingham en considérant des conditions de glissement aux parois. L'effet du coefficient de frottement sans dimension C_f est mis en évidence. Lorsque $C_f < O(1)$, le nombre de Rayleigh critique Ra_c tend vers le cas libre-libre ; pour $10 < C_f < 30$, les valeurs de Ra_c atteignent un minimum ; pour $C_f > 30$ l'écoulement est stabilisé ; finalement le cas rigide-rigide est retrouvé pour $C_f > 1000$ en terme de valeurs de Ra_c. Par ailleurs, des modes dissymétriques sont observés lorsque $1 < C_f < 10^4$.

Abstract :

A linear stability analysis is performed for the Rayleigh-Bénard Poiseuille flow for a Bingham fluid and considering slip boundary conditions at walls. The influence of the friction number C_f is investigated. When $C_f < O(1)$, the critical Rayleigh number Ra_c tends to that of the free-free case ($C_f \to 0$; for $10 < C_f < 30$, the Ra_c values reach a minimum ; for $C_f > 30$ the flow is stabilized ; finally the rigid-rigid case is recovered for $C_f > 1000$, in terms of Ra_c. Furthermore, asymmetric modes are observed for $1 < C_f < 10^4$.

Mots clefs : **Yield stress fluids ; slip at walls ; thermoconvective instabilities**

1 Introduction

Slip occurs in flows of concentrated dispersions due to the displacement of the disperse phase away from solid walls. Slip effects are usually observed when the disperse phase presents a multi-micron size of particles or of droplet (emulsion). When sheared with smooth surfaces, the concentrated dispersions exhibit apparent motion. Reviews on this topic have been proposed by Oldroyd (1) and Barnes (2). Due to its practical interest, the slip of non-Newtonian fluids is widely studied. In particular, the slip of polymer microgels in rheometers is studied for a long time (e.g. (3)-(5)).

The aim of this paper is to study the effect of slip near solid surfaces on the instability conditions when a viscoplastic fluid is involved. In particular, we propose to study the Rayleigh-Bénard Poiseuille (RBP) flow of a Bingham fluid. In the present paper, we propose to extend the study of (6) considering slip conditions at walls.

2 Governing equations

We consider the plane Poiseuille flow under an imposed axial pressure gradient of a yield stress fluid in a horizontal plane channel. The upper and lower walls are at constant temperatures, $\widehat{T}_0 - \delta\widehat{T}/2$ and $\widehat{T}_0 + \delta\widehat{T}/2$, respectively. The hat notation is used for all dimensional variables. The dimensionless problem is obtained using the width $\widehat{L}$ of the plane channel as length-scale, and the thermal diffusion time $\widehat{L}^2/\widehat{a}$ between the two walls as the timescale; here $\widehat{a}$ is the thermal diffusivity of the fluid. The

velocity scale is the maximum velocity $\widehat{U}_0$ of the no-slip boundary conditions. With the Boussinesq approximation, the governing equations read:

$$\boldsymbol{\nabla}\cdot\boldsymbol{U}=0, \tag{1a}$$

$$Re\,\boldsymbol{U}_t+Re^2\,Pr\,(\boldsymbol{U}\cdot\boldsymbol{\nabla})\,\boldsymbol{U}=Re\,Pr\,(-\boldsymbol{\nabla}P+\boldsymbol{\nabla}\cdot\boldsymbol{\tau})+Ra\,T\,\boldsymbol{e_y}\,, \tag{1b}$$

$$T_t+Re\,Pr\,(\boldsymbol{U}\cdot\boldsymbol{\nabla})\,T=\nabla^2 T, \tag{1c}$$

The velocity vector $\boldsymbol{U}$ is of the form $\boldsymbol{U}=U\,\boldsymbol{e}_{\rm x}+V\,\boldsymbol{e}_{\rm y}$, where U and V are the velocity components and $\mathbf{e}_{\rm x},\mathbf{e}_{\rm y}$ are unit vectors in the streamwise and transverse directions, respectively.

The dimensionless numbers are the Reynolds, $Re=\dfrac{\widehat{\rho}\widehat{U}_0\widehat{L}}{\widehat{\mu}_0}$, Prandtl, $Pr=\dfrac{\widehat{\mu}_0\widehat{a}}{\widehat{\rho}}$ and Rayleigh, $Ra=\dfrac{\widehat{\rho}\widehat{\alpha_0}\widehat{g}\delta\widehat{T}\widehat{L}^3}{\widehat{\mu}_0\widehat{a}}$ numbers, $\widehat{\rho}$ is the fluid density, $\widehat{\alpha_0}$ is the thermal expansion coefficient and $\widehat{g}$ the gravitational acceleration.

The constitutive law for a Bingham fluid is given by:

$$\boldsymbol{\tau} = \mu\dot{\boldsymbol{\gamma}} \qquad \text{iff} \quad \tau>B, \tag{2}$$

$$\dot{\gamma} = 0 \qquad \text{iff} \quad \tau\le B, \tag{3}$$

with $\mu=\mu_0+\dfrac{B}{\dot{\gamma}}$ the effective viscosity and $B=\widehat{\tau}_0\,\widehat{L}/\left(\widehat{\mu}_0\,\widehat{U}_0\right)$ the Bingham number. The rate of strain tensor is denoted by $\dot{\boldsymbol{\gamma}}$; $\dot{\gamma}$ and τ are the second invariants of the rate of strain and deviatoric stress tensors, respectively.

The set (1) is completed by the boundary conditions at walls:

$$T(-1/2)=T_1=1/2 \quad \text{and} \quad T(1/2)=T_2=-1/2, \tag{4}$$

$$V(\pm1/2) = 0, \tag{5}$$

$$U(\pm1/2) = -\frac{\tau_{xy}(\pm1/2)}{C_f}\left[1-\frac{S}{\tau_{xy}(\pm1/2)}\right] \qquad \text{if} \quad |\tau_{xy}(\pm1/2)|>S, \tag{6}$$

$$U(\pm1/2) = 0 \qquad \text{if} \quad |\tau_{xy}(\pm1/2)|\le S, \tag{7}$$

with $S=\dfrac{\widehat{s}_0\widehat{L}}{\widehat{\mu}_0\widehat{U}_0}$ the slip yield number and $C_f=\dfrac{\widehat{c}_f\widehat{L}}{\widehat{\mu}_0}$ the friction number, $\widehat{s}_0$ the yield stress when slip occurs at walls and $\widehat{c}_f$ the friction dissipation coefficient.

The steady state flow leads to a basic conductive state and the velocity $\boldsymbol{U}_b=(U_b(y),0,0)$ reads:

$$U_b(y)=\begin{cases} 1+\dfrac{1}{C_f}\left(\dfrac{B}{2y_b}+S\right) & \text{for} \quad |y|\le y_b \\ 1-\left(\dfrac{|y|-y_b}{1/2-y_b}\right)^2+\dfrac{1}{C_f}\left(\dfrac{B}{2y_b}+S\right) & \text{for} \quad y_b<|y|<1/2, \end{cases} \tag{8}$$

where $2y_b$ is the width of the central unyielded region as shown in Fig. 1 (gray region) and given by the relation $B=(2y_b)/(y_b-1/2)^2$. Velocity profiles are displayed in Fig. 1 by varying S and C_f values.

The limit case $C_f\to 0$ is denoted as the free-free case in the following. The distinction is made with the perfect slip case. Indeed, the perfect slip case leads to an entire unyielded flow which is linearly stable.

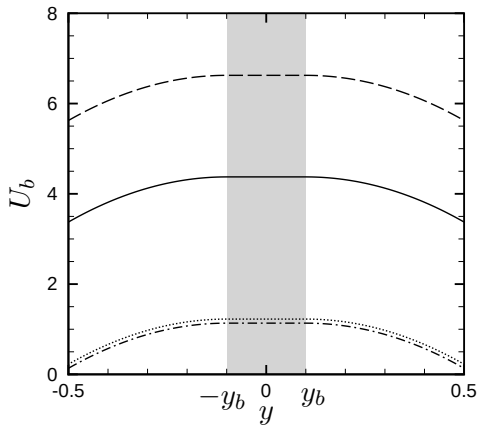

Figure 1: Velocity profiles for $y_b = 0.1$ ($B = 1.25$) and different values of C_f and S. The gray zone represents the unyielded region. Dotted lines: $S = 5, C_f = 50$, dashed lines: $S = 5, C_f = 2$, dash-dotted lines: $S = 0.5, C_f = 50$, solid lines: $S = 0.5, C_f = 2$.

3 Linear stability analysis

One introduces a small perturbation $A(\psi, \Theta, p, \pm y_i^{\pm})$ to the fully developed flow. Here, A corresponds to the amplitude of the perturbation and ψ is the stream function, defined by $u = \partial_y \psi$ and $v = -\partial_x \psi$. The perturbations field is sought in the following form:

$$\big(\psi,\, \pm y_i^{\pm},\, p,\, \Theta\big) = \big(f(y),\, \pm y_1^{\pm},\, p(y),\, \theta(y)\big)\, e^{\mathrm{i}\,\alpha\,(x-ct)}, \tag{9}$$

where α denotes the streamwise wave number and $\alpha c_i = Im(\omega)$ denotes the growth rate, with $\omega = \alpha\, c$. Considering Eq. (9), the linearized equations of perturbations read in the yielded regions as follows:

$$\mathcal{L}_1 f + \mathcal{L}_2 \theta = c\, \mathcal{L}_3 f, \tag{10a}$$

$$\mathcal{L}_4\, \theta + f = c\, \theta, \tag{10b}$$

with $\mathcal{L}_1, \mathcal{L}_2$, $\mathcal{L}_3$ and $\mathcal{L}_4$, the following operators:

$$\begin{aligned}
\mathcal{L}_1 \equiv & Pr\, Re \left[U_b(D^2 - \alpha^2) - D^2 U_b\right] + \frac{Pr\mathrm{i}}{\alpha}(D^2 - \alpha^2)^2 - 4\,\mathrm{i}\,\alpha\, Pr\, B\, D \left[\frac{D}{|DU_b|}\right], \\
\mathcal{L}_2 \equiv & Pr\, Ra, \\
\mathcal{L}_3 \equiv & D^2 - \alpha^2, \\
\mathcal{L}_4 \equiv & Pr\, Re\, U_b - i\alpha + \frac{i}{\alpha} D^2,
\end{aligned} \tag{11}$$

where $D \equiv \partial_y$. In the unyielded region, the eigenvalue problem is reduced to:

$$f = 0, \tag{12a}$$

$$\mathcal{L}_4\, \theta = c\, \theta. \tag{12b}$$

At the yield surfaces ($y = y_i^{\pm}$), the yield conditions lead to:

$$f(\pm y_b) = \partial_y f(\pm y_b) = 0 \tag{13}$$

At the walls ($y = \pm 1/2$), the boundary conditions read:

$$\theta(\pm 1/2) = 0, \tag{14}$$

$$\left[\partial_{yy} f + C_f\, \partial_y f - \alpha^2 f\right]_{\pm 1/2} = 0, \tag{15}$$

$$v(\pm 1/2) = -f(\pm 1/2) = 0. \tag{16}$$

As a remark, one can notice that S does not have any influence on the stability analysis (Eqs (10)-(16)).

4 Results and discussion

The set of equations (10)-(16) is solved numerically by means of a finite differences method. A second-order centered finite scheme is used in order to discretize the equations. The resulting problem represents an eigenvalue problem which is solved using the QZ algorithm implemented in Matlab 7.1. In this work, the convergence of the results is obtained for $N = 301$.

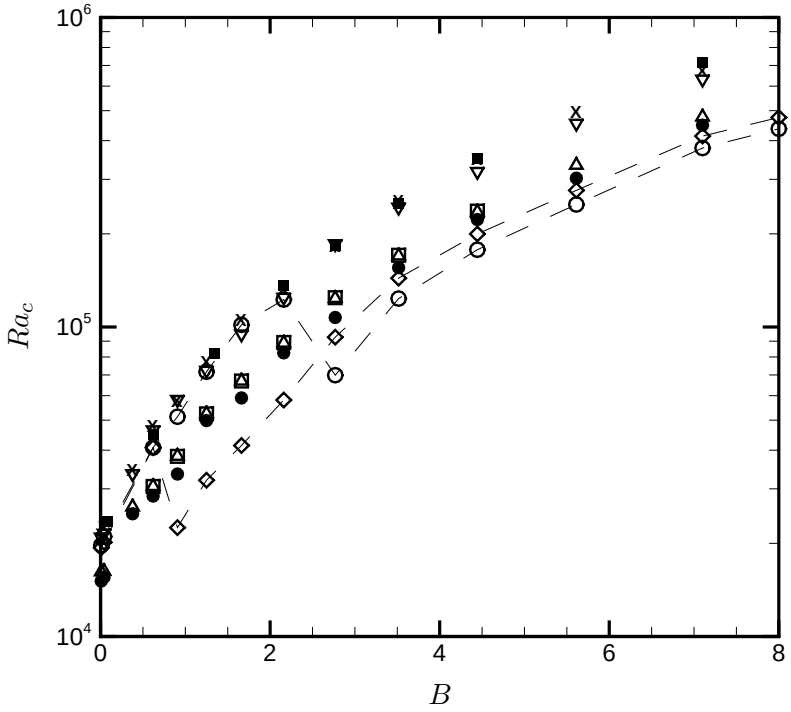

Figure 2: Evolution of the critical Rayleigh number as function of the Bingham number for different values of the friction number C_f and $S = 2$, $Re = 0.01$ (Black squares: No-slip case, Squares: $C_f = 0.001$, Deltas: $C_f = 0.01$, Black circles: $C_f = 5$, Diamonds: $C_f = 15$, Circles: $C_f = 20$, Gradients: $C_f = 50$, Crosses: $C_f = 100$).

The Figure 2 represents critical conditions for different values of the friction number C_f with $S = 2$. This value of S involves cases for which the fluid slips at walls, for all B. Slip conditions at walls destabilize the flow since the Ra_c values are smaller than that of the no-slip case (black squares). When $C_f > 30$, critical conditions tend to that obtained in the no-slip case while for $C_f < 10$, Ra_c values tend to the free-free case. A transition region is observed for $10 < C_f < 30$. Actually, in this range of values, one observes that (i) if $B < B_c$, B_c a critical value, then Ra_c values tend to the no-slip conditions, (ii) if $B > B_c$, a large variation is observed in Ra_c and the flow is destabilized as given in Fig. 2 (see circles and diamonds symbols with dashed lines). Furthermore, one observes that B_c varies slightly with C_f as it is also underlined in Fig. 3 (dashed lines). In Fig. 3, one notices that, for fixed values of B, Ra_c is constant when $C_f < O(1)$ and is equal to the value obtained for the limit case $C_f \to 0$. For $10 < C_f < 30$, values of Ra_c decrease, reach a minimum at $C_{fm} = 0(10)$ and then increase significantly. Finally, Ra_c values tend to that of the no-slip case for large values of C_f ($C_f > 50$). Figures 2 and 3 show clearly that the transition between the free-free and the no-slip cases is abrupt and depends on C_f values. In order to underline this dependency, calculations have been performed setting artificially $C_f = 0$ only in the boundary conditions (15), i.e. for each value of C_f the basic flow is retained but perturbation boundary conditions at walls are modified. We have observed that for all tested values of C_f, critical conditions obtained are similar to that of the case $C_f = 0.001$.

It means that any variation with C_f in criticality (spectra, eigenmodes, critical conditions) is only due to the competition between the free-free case and the no-slip case via the value of C_f in Eq. (15).

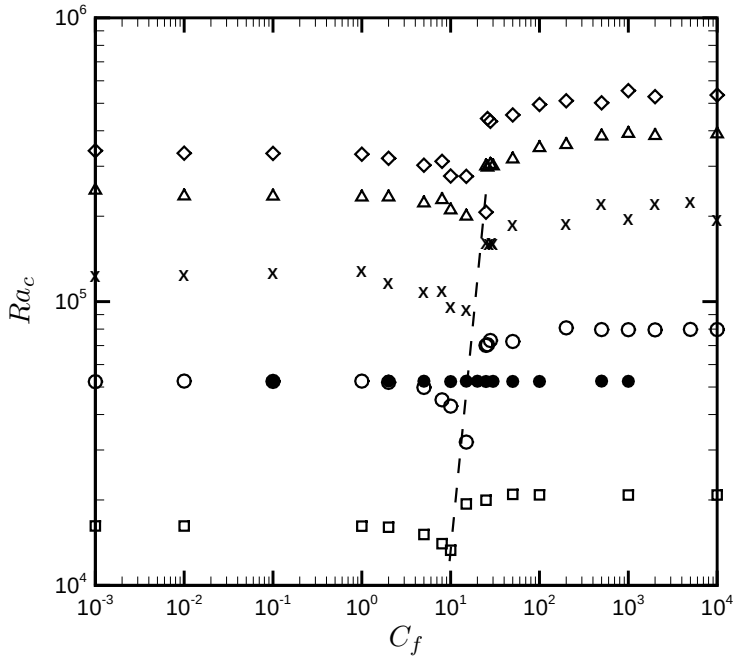

Figure 3: Evolution of the critical Rayleigh number as function of the friction number C_f and $S = 2$, $Re = 0.01$ (Squares: $y_b = 0.001$ ($B = 0.008$), Circles: $y_b = 0.1$ ($B = 1.25$), Black Circles: $y_b = 0.1$ and $C_f = 0$ in Eq. (15), Crosses: $y_b = 0.16$ ($B = 2.77$), Deltas: $y_b = 0.2$ ($B = 4.44$), Diamonds: $y_b = 0.22$ ($B = 5.61$). The dashed line indicates the minimal values of Ra_c.

The structure of the perturbed flow can be represented by the least stable mode in terms of temperature and stream function as given by Figs. 4-5.

The asymptotic cases are compared in Fig. 4 since critical modes are displayed for the no-slip case (solid line) and the free-free case (dashed line). One can observe the main difference between these two cases via the derivative of f at walls according to different boundary conditions.

For $1 < C_f < 10^4$, one can notice asymmetric modes as represented in Fig. 5. The increase in C_f values increases the differences between the extrema of the modes in the two yielded regions. The symmetry of the critical modes are finally found for large values of C_f, i.e. $C_f = 10000$. For this value of C_f, critical modes tend to the no-slip case ones.

References

[1] Oldroyd J.G, Non-Newtonian flow of solids and liquids. *In Eirich F.R. (editor), Rheology: Theory and applications Vol.* ***1***, Academic Press Inc., New York (1956) 653-682.

[2] H.A. Barnes, A review of the slip (wall depletion) of polymers solutions, emulsions and particle suspensions in viscosimeters: it causes, character, and cure. *J. Non-Newtonian Fluid Mech.* **36** (1995) 85-108.

[3] G.V. Vinogradov & G.B. Froisheter & K.K. Trilisky, The flow of plastic disperse systems in the presence of the wall effect. Rheol. Acta, **14** 9 (1975) 765.

[4] A. Magnin & J.M. Piau, Cone-and-plate rheometry of yield stress fluids. Study of an aqueous gel. J. Non-Newtonian Fluid Mech., **56** (1990) 221-251.

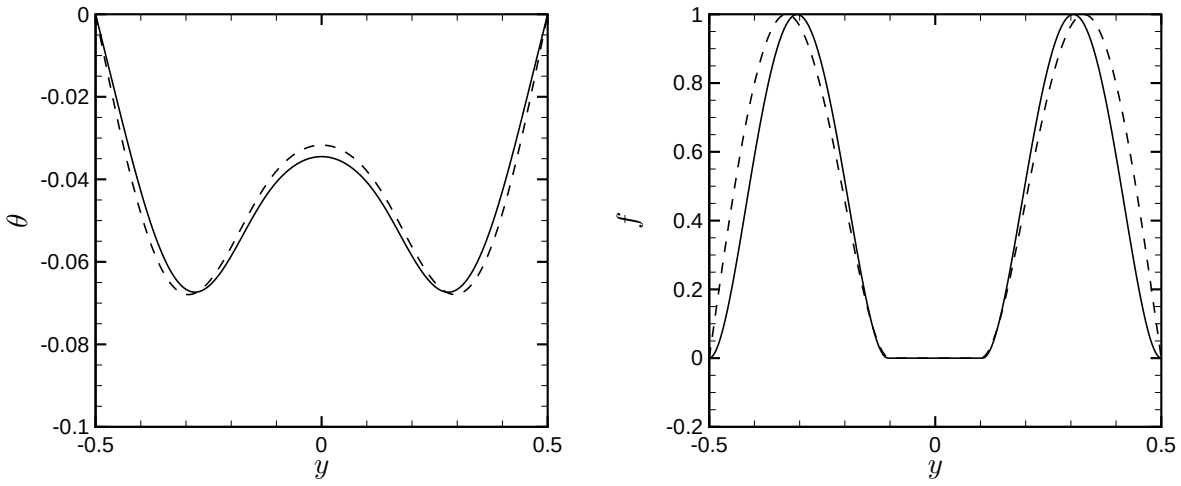

(a) Temperature (imaginary part) (b) Stream function (real part)

Figure 4: Critical modes for the no-slip case, $y_b = 0.1$ ($B = 1.25$), $Re = 0.01$ (solid line: no-slip case, dashed line: $C_f = 0.001$ (free-free case)).

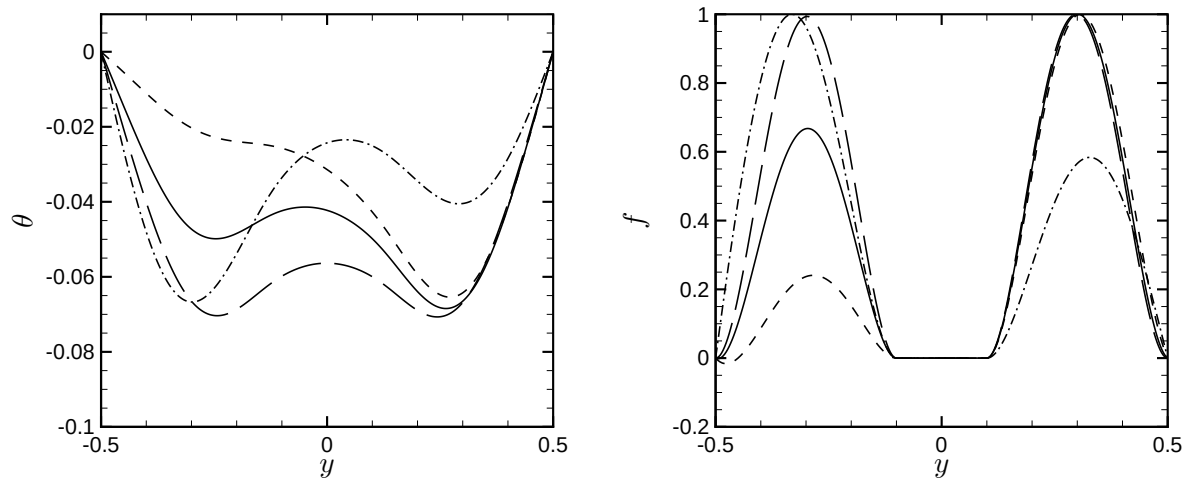

(a) Temperature - Imaginary part (b) Stream function - Real part

Figure 5: Critical modes for different values of C_f, $S = 2$, $y_b = 0.1$ ($B = 1.25$), $Re = 0.01$ (Long dashed line: $C_f = 10000$, solid line: $C_f = 200$, dashed line: $C_f = 50$, dash-dotted line: $C_f = 1$).

[5] J.M. Piau, Carbopol gels: Elastoviscoplastic and slippery glasses made of individual swollen sponges. Meso- and macroscopic properties, constitutive equations and scaling laws J. Non-Newtonian Fluid Mech., **144** (2007) 1-29.

[6] C. Métivier & C. Nouar, On linear stability of Rayleigh-Bénard Poiseuille flow of viscoplastic fluids. *Phys. Fluids* **20** (10) (2008).